Can the Benjamin-Feir instability spawn a rogue wave?

H. Segur[1], D. M. Henderson[2], and J. L. Hammack (1944-2004)

[1]Department of Applied Mathematics, University of Colorado, Boulder, CO 80304 USA

[2]Department of Mathematics, Pennsylvania State University, University Park PA 16802 USA

Abstract. Recent work by our research group has shown that wave damping can have a surprisingly strong effect on the evolution of waves in deep water, even when the damping is weak. Whether damping is or is not included in a theoretical model can change the outcome in terms of both stability of wave patterns and frequency downshifting. It is conceivable that it might affect the early development of rogue waves as well.

1. Introduction and summary of results

Rogue waves have long been part of sailing lore, but only in recent years have oceanographers accepted the challenge of providing accurate models to describe and to predict these dangerous ocean waves. These Proceedings are evidence of the heightened interest by oceanographers in rogue waves.

In some theoretical models, including some presented in these Proceedings, the development of a rogue wave begins when uncorrelated waves happen to focus their energy in a highly localized region of the sea. In these models, the initial focusing is often described by the well-known nonlinear Schrödinger (NLS) equation. As the size and steepness of the waves develop, the process eventually leaves the range of validity of NLS, and full nonlinear dynamics take over. Even so, the crucial first stages of the focusing process are governed by NLS dynamics in these models.

Our recent experimental and theoretical work has identified the important role that wave damping can play in the dynamics of deep-water waves, even when the damping is weak. Wave damping is neglected in standard NLS models, and we have found that adding damping to an NLS-type model can significantly improve the accuracy of the model.

As a striking example of the importance of wave damping, Figure 1 shows a laboratory experiment in which two one-dimensional wavetrains interact obliquely and produce a two-dimensional pattern of surface waves that propagates with nearly permanent form in deep water. The wave pattern is approximately periodic in two spatial directions, and it maintains that form as it propagates. One might expect a wave pattern like this to break up in deep water due to a modulational instability, like that studied by *Benjamin and Feir* (1967). But the wave pattern in Figure 1 shows no evidence of instability within the test section of the wave tank.

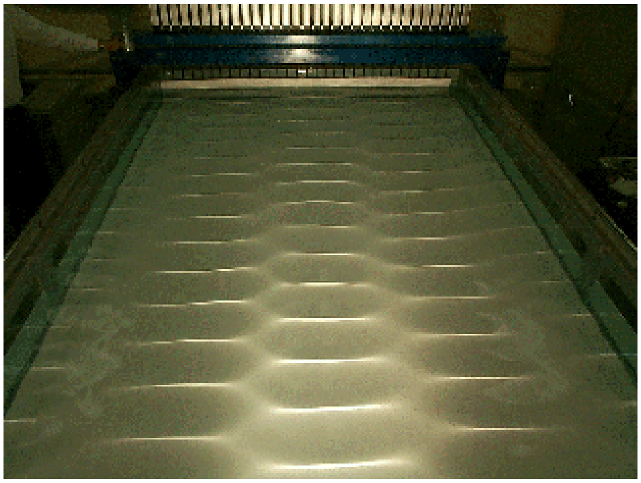

Figure 1. An oblique interaction of two, one-dimensional wavetrains in deep water produces this two-dimensional pattern that propagates away from the array of paddles at the top of the picture with nearly permanent form, and with no evidence of instability within the test section of the wave. These waves have a frequency of 2 Hz, in water of depth 20 cm. (For more information on persistent, two-dimensional, periodic wave patterns in deep water, see http://www.math.psu.edu/dmh/FRG/.)

Hammack et al. (2005) showed that the dynamics of this two-dimensional surface pattern can be modeled approximately with a coupled pair of nonlinear

Schrödinger equations, and one can choose either to include or to exclude damping in the model. The model without damping predicts that this wave pattern is *unstable* to a Benjamin-Feir kind of instability, while the model with damping predicts the same wave pattern is *stable*. We are now preparing to compare both sets of predictions with experimental data (Bleymaier, Henderson, and Segur, in preparation.)

We have made detailed comparisons of theoretical predictions with experimental data in a simpler problem: periodic waves in deep water with one-dimensional surface patterns (i.e., plane waves), like those studied by *Benjamin and Feir* (1967) and *Lake et al.* (1977). For plane waves, the same dichotomy occurs between NLS models with and without damping. *Zakharov* (1968) showed that the NLS model with no damping predicts that a uniform train of monochromatic waves of moderate amplitude is unstable in deep water, while *Segur et al.* (2005) showed that any finite amount of damping (of the right kind) stabilizes the instability. For plane waves, extensive comparisons of theory with experimental data show that the damped model predicts the observed behaviour of these waves in deep water much more accurately than does the undamped model. A summary of these results is given in sections 3 and 4 of t*his paper. (See Segur et al., 2005 for full details, and see Hammack et al.*, 2005 for experimental results on wave pattern like those shown in Figure 1.)

These results about the stability of periodic wave patterns apply to waves of small or moderate amplitude in deep water. For deep-water waves of larger amplitude or with larger perturbations, we find that neither the usual NLS equation, the damped NLS equation, nor higher order versions of the NLS equation predicts our experimental data accurately, because these models fail to predict *frequency downshifting*. *Lake et al.* (1977) first observed downshifting, in which the dominant frequency of a uniform wavetrain gradually shifts to a lower value. We regard frequency downshifting as a nolinear, dissipative process that is not yet well understood. We show in section 5 that neither the standard NLS model, its higher order version, nor the damped NLS model describes downshifting accurately.

Now let us return to rogue waves, and to the theoretical models of these waves that begin with wave focusing in an NLS model. Our recent results (summarized in this paper) show that the NLS equation should be modified to include wave damping in order to obtain accurate results for the stability of deep-water waves of small or moderate amplitude, even if the damping is small. We also find that the NLS model needs to be modified in some (still unknown) way to describe correctly the downshifting that is observed for deep-water waves with more energetic perturbations. Either or both of these dissipative processes might also affect the early development of rogue waves. These possibilities apply to the non-dissipative NLS equation, but they also apply to the more accurate but also non-dissipative Euler equations. Our main point at this time is cautionary. We have no experimental evidence on how or to what extent dissipation affects the early development of rogue waves.

2. Nonlinear Schrödinger models of waves in deep water

The derivation of the nonlinear Schrödinger equation as an approximate model of the evolution of nearly monochromatic waves of moderate amplitude in deep water without dissipation can be found in many places (*e.g.*, *Zakharov*, 1968, *Ablowitz and Segu*r, 1981), so we simply state results here. Let $\{X,Y\}$ represent coordinates on a horizontal plane, let T represent time, and let $\varepsilon > 0$ be a formal small parameter. For nearly monochromatic waves of small amplitude, propagating primarily in one direction, one can represent the vertical displacement of the water's free surface in the form

$$\eta(X,Y,T;\varepsilon) = \varepsilon[\psi(x,y,t)e^{i\theta} + \psi^* e^{-i\theta}] + \varepsilon^2[\psi_2(x,y,t)e^{2i\theta} + \psi_2^* e^{-2i\theta}] + O(\varepsilon^3) \tag{2.1}$$

where

- $\theta = k_0 X - \omega(k_0)T$ represents the fast oscillation of a carrier wave,
- $\omega(k)$ is the linearized dispersion relation, so $\omega^2 = gk$ for inviscid waves in deep water under the influence of gravity (g),
- $x = \varepsilon\omega(k_0)\cdot(T - X/c_g)$ and $y = \varepsilon k_0 Y$ are coordinates to describe the slow modulation of the wave envelope in a coordinate system moving with speed $c_g = \frac{d\omega}{dk}$, and
- $t = \varepsilon^2 k_0 X$ is the time-like variable in which to observe the slow evolution of the envelope as it propagates down the tank.

For irrotational motion, the velocity potential has a corresponding expansion. One substitutes these expansions into the governing equations for the motion of an incompressible, inviscid fluid with a free surface, under the influence of a constant gravitational field (g), and solves order-by-order in ε. The first nonlinear effect is that

$$\psi_2(x,y,t) = k_0[\psi(x,y,t)]^2\,, \tag{2.2}$$

as first discovered by *Stokes* (1847). In addition, $\psi(x,y,t)$ must satisfy approximately the nonlinear Schrödinger (NLS) equation, in the form

$$i\partial_t\psi - \partial_x^2\psi + \frac{1}{2}\partial_y^2\psi - 4k_0^2\,|\psi|^2\,\psi = 0\,. \tag{2.3}$$

Thus, ψ represents the complex amplitude of a slowly varying train of waves of finite amplitude, and (2.3) describes approximately the slow evolution of that amplitude as the waves propagate primarily in the X-direction. For later purposes, we note that the coordinate system used in (2.3) is appropriate for waves that propagate away from a controlled source: the time-like variable is proportional to the distance the wave has propagated from the source (X), while (T) becomes space-like.

The NLS model in (2.3) neglects wave damping altogether. To examine the effect of weak damping, we also consider a dissipative generalization of (2.3):

$$i\partial_t\psi - \partial_x^2\psi + \frac{1}{2}\partial_y^2\psi - 4k_0^2\,|\psi|^2\,\psi + i\delta\psi = 0\,, \tag{2.4}$$

where $\delta \geq 0$ represents wave damping. *Miles* (1967) reviewed and derived analytic formulae for δ, based on various kinds of physical dissipation that affect waves in deep water. In this paper we regard δ as an empirical parameter, which we measure directly for each set of experiments.

For definiteness, we seek solutions of either (2.3) or (2.4) on a rectangular domain D, with periodic conditions on the boundaries of D. Then (2.3) admits integral constants of the motion, including

$$M = \frac{1}{A_D}\iint_D |\psi(x,y,t)|^2 dxdy\,,$$

and
$$\boldsymbol{P} = \frac{i}{A_D}\iint_D [\psi\nabla\psi^* - \psi^*\nabla\psi]dxdy\,, \tag{2.5}$$

where ()* denotes complex conjugate, $\nabla\psi = (\partial_x\psi, \partial_y\psi)$, and A_D is the area of the domain. Sometimes M is called "mass" or "wave energy", and the two components of $\boldsymbol{P}$ are called "linear momentum" (cf. *Sulem and Sulem*, 1999). For (2.4) with $\delta > 0$, these quantities vary in time, but in a simple way:

$$M(t) = M(0)\cdot\exp(-2\delta t)$$

$$\boldsymbol{P}(t) = \boldsymbol{P}(0)\cdot\exp(-2\delta t) \tag{2.6}$$

The forms in (2.6) suggest a change of variables:

$$\psi(x,y,t) = \mu(x,y,t)\cdot\exp(-\delta t)\,. \tag{2.7}$$

After this change, (2.4) becomes

$$i\partial_t\mu - \partial_x^2\mu + \frac{1}{2}\partial_y^2\mu - 4k_0^2 e^{-2\delta t}\,|\mu|^2\,\mu = 0\,. \tag{2.8}$$

For $t > 0$, (2.6) shows that $\psi \to 0$ in L$_2$-norm, but (2.7) factors out this overall decay. With periodic boundary conditions on D, (2.8) admits constants of the motion:

$$M_\mu = \frac{1}{A_D}\iint_D |\mu(x,y,t)|^2\,dxdy = const\,, \tag{2.9a}$$

$$\boldsymbol{P}_\mu = \frac{i}{A_D}\iint_D [\mu\nabla\mu^* - \mu^*\nabla\mu]dxdy = const\,. \tag{2.9b}$$

In addition, (2.8) is a Hamiltonian system, with conjugate variables $\{\mu, \mu^*\}$ and Hamiltonian

$$H_\mu = i\iint_D [-|\partial_x\mu|^2 + \frac{1}{2}|\partial_y\mu|^2 + 2k_0^2 e^{-2\delta t}\,|\mu|^4]dxdy\,. \tag{2.10}$$

This Hamiltonian is not a constant of the motion unless δ = 0, but it is noteworthy that (2.8) is a Hamiltonian equation that describes a naturally occurring dissipative process. If δ = 0, then (2.8) reduces to (2.3), and (2.10) reduces to the Hamiltonian for (2.3).

3. Stability of a uniform wavetrain in deep water

Including wave damping in the NLS model has a striking effect on stability, even when the damping is weak. *Benjamin and Feir* (1967), *Zakharov* (1968), and others established a fundamental principle of nonlinear wave dynamics, when they discovered that a uniform train of periodic plane waves (*i.e.*, with one-dimensional surface patterns) of moderate amplitude is unstable in deep water without damping. The (rapid) carrier wave oscillation has been factored out of the NLS model, so a uniform train of periodic plane water waves is represented by a spatially constant solution of (2.3),

$$\psi_0(t) = A\cdot\exp\{-4ik_0^2\,|A|^2\,t\}\,, \tag{3.1}$$

where $\{A\}$ is a complex constant. Following *Zakharov* (1968), one examines the linear stability of such a solution by linearizing (2.3) around this solution,

$$\psi(x,y,t) = e^{-4ik_0^2|A|^2 t + i\arg(A)}\{|A| + \zeta\cdot u(x,y,t)$$

$$+ i\zeta\cdot v(x,y,t) + O(\zeta^2)\} \tag{3.2}$$

and retaining only terms linear in ζ. The result is a pair of linear partial differential equations for $\{u, v\}$. These equations have constant coefficients, so one may seek solutions of the form

$$u(x,y,t) = U(m,l,\Omega)\cdot e^{imx+ily+\Omega t} + (c.c.)$$

$$v(x,y,t) = V(m,l,\Omega)\cdot e^{imx+ily+\Omega t} + (c.c.)\,,$$

where (*c.c.*) denotes complex conjugate. The solution in (3.1) is linearly unstable if there is an allowable (*m,l*) for which $\mathrm{Re}\{\Omega(m,l)\} > 0$. One finds that $\Omega(m,l)$ satisfies

$$\Omega^2 + (-m^2 + \frac{l^2}{2})\cdot(-m^2 + \frac{l^2}{2} + 8k_0^2\,|A|^2) = 0\,. \tag{3.3}$$

The first factor in the product vanishes along two straight lines in the (*m,l*) plane, while the second vanishes on a hyperbola with these straight lines as asymptotes. Any choice of (*m,l*) that lies between these two sets of curves is unstable, as shown in Figure 2. For a wavetrain with finite amplitude *A*, there is always a finite range of unstable wavenumbers, so every such wavetrain is unstable in a large enough domain *D*. This is the famous modulational (or Benjamin-Feir) instability, as it appears in the NLS model.

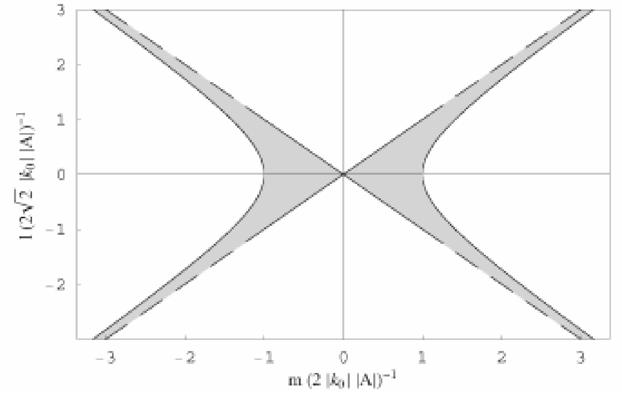

Figure 2. Stability space as defined by (3.3), with δ = 0. Any {m, l} in the shaded region corresponds to a linearly unstable mode.

When damping is included, as in (2.4) or (2.8), the stability analysis of a uniform wavetrain follows similar lines, but the outcome is strikingly different. With damping, a uniform train of plane periodic waves in deep water is represented by a spatially constant solution of (2.4) of the form

$$\psi_0(t) = Ae^{-\delta t}\exp\{-4ik_0^2\,|A|^2\,(\frac{1-e^{-2\delta t}}{2\delta})\}\,, \tag{3.4a}$$

where $\{A\}$ is a complex constant. The equivalent solution of (2.8) is

$$\mu_0(t) = A\exp\{-4ik_0^2\,|A|^2\,(\frac{1-e^{-2\delta t}}{2\delta})\}\,. \tag{3.4b}$$

One examines the linearized stability of the solution in (3.4b) by linearizing (2.8) around it,

$$\begin{aligned}\mu(x,y,t) &= \exp\{-4ik_0^2\,|A|^2\,(\frac{1-e^{-2\delta t}}{2\delta}) + i\arg(A)\}\cdot\\ &\quad\{|A| + \zeta\cdot u(x,y,t) + i\zeta\cdot v(x,y,t) + O(\zeta^2)\},\end{aligned} \tag{3.5}$$

retaining only terms linear in ζ. The result is a pair of linear partial differential equations for (*u,v*),

$$\begin{aligned}\partial_t v &= -\partial_x^2 u + \frac{1}{2}\partial_y^2 u - 8k_0^2 e^{-2\delta t}\,|A|^2\,u,\\ -\partial_t u &= -\partial_x^2 v + \frac{1}{2}\partial_y^2 v.\end{aligned} \tag{3.6}$$

From (2.6), all square-integrable solutions of (2.4) decay to zero as $t \to \infty$. This overall decay has been factored out of (2.8), so a spatially constant solution like that in (3.4) is unstable if perturbations (*u,v*) grow without bound relative to the constant amplitude, |*A*|; the growth rate of the instability is not required to exceed the overall decay rate, $e^{-\delta t}$.

Equations (3.6) have constant coefficients in (*x,y*) but not in (*t*), so one may seek solutions of (3.6) in the form of a Fourier mode:

$$u(x,y,t) = U(t;m,l)\cdot e^{imx+ily} + (c.c.)\,, \tag{3.7a}$$

$$v(x,y,t) = V(t;m,l)\cdot e^{imx+ily} + (c.c.)\,. \tag{3.7b}$$

Then (3.6) becomes

$$\frac{dV}{dt} = -(-m^2 + \frac{l^2}{2} + 4k_0^2 e^{-2\delta t}\,|A|^2)U\,, \tag{3.8a}$$

$$\frac{dU}{dt} = (-m^2 + \frac{l^2}{2})V\,, \tag{3.8b}$$

or (3.4b)

$$\frac{d^2U}{dt^2} + [(-m^2 + \frac{l^2}{2})(-m^2 + \frac{l^2}{2} + 8k_0^2 e^{-2\delta t}\,|A|^2)]U = 0\,. \tag{3.8c}$$

Equation (3.8) is a Sturm-Liouville problem (*cf. Ince*, 1956, Ch. 10), so Sturmian theory implies the following results:

if $[(-m^2 + \frac{l^2}{2})(-m^2 + \frac{l^2}{2} + 8k_0^2 e^{-2\delta t}\,|A|^2)] > 0$,

all solutions of (3.8) oscillate in time;

if $[(-m^2+\frac{l^2}{2})(-m^2+\frac{l^2}{2}+8k_0^2e^{-2\delta t}\,|A|^2)]<0$, then (3.8) admits a growing solution. As long as $[(-m^2+\frac{l^2}{2})(-m^2+\frac{l^2}{2}+8k_0^2e^{-2\delta t}\,|A|^2)]\le -C^2<0$, this solution grows at least as fast as $e^{|C|t}$.

Here is the fundamental reason for the difference in stability between the spatially constant solutions of (2.3) and (2.8). According to (3.8), at any fixed time the set of (*m,l*)-modes that can grow exponentially lie in a region like that shown in Figure 2. However, the bounding hyperbola for (2.8) is defined by

$$-m^2+\frac{l^2}{2}+8k_0^2e^{-2\delta t}\,|A|^2=0\,, \tag{3.9}$$

so the region of instability shrinks as *t* increases, and any specific (*m,l*)-mode resides in this shrinking region only for a limited time. After that time, every solution of (3.8) for this (*m,l*) oscillates in time. No (*m,l*)-mode grows forever. In addition, the total growth of any (*m,l*)-mode is finite. One can show that for any (*m,l*), any $\delta > 0$ and any $t \ge 0$, the solution of (3.8) necessarily satisfies

$$\begin{aligned}|U(t;m,l)| &\le \sqrt{|U(0;m,l)|^2+|V(0;m,l)|^2}\cdot\exp\{\frac{4k_0^2\cdot|A|^2}{\delta}(1-e^{-2\delta t})\},\\ |V(t;m,l)| &\le \sqrt{|U(0;m,l)|^2+|V(0;m,l)|^2}\cdot\exp\{\frac{4k_0^2\cdot|A|^2}{\delta}(1-e^{-2\delta t})\}.\end{aligned} \tag{3.10}$$

Therefore, if $\delta > 0$ then for all $t \ge 0$, every (*m,l*)-mode satisfie

$$|U(t)|^2+|V(t)|^2\le 2[\{|U(0)|^2+|V(0)|^2\}\exp\{\frac{8k_0^2\cdot|A|^2}{\delta}(1-e^{-2\delta t})\}] \tag{3.11}$$

What does "stability" mean? For a Hamiltonian system like (2.3) or (2.8), we say that a solution is stable if every other solution of the equation that starts close to it (at t = 0) stays close to it for all t > 0. This is sometimes called Lyapunov stability (cf. *Nemytskii and Stepanov*, 1960). To make this precise for the solution of (2.8) in (3.4b), let {*u(x,y,t)*, *v(x,y,t)*} represent any solution of (3.6), with initial data {*u(x,y*,0), *v(x,y*,0)}. We say that $\mu_0(t)$ in (3.4b) is a linearly stable solution of (2.8) if for every ε > 0 there is a Δ(ε) > 0 such that if, at *t*=0,

$$\iint_D [|u(x,y,0)|^2+|v(x,y,0)|^2]\;dxdy<\Delta\,, \tag{3.12a}$$

then necessarily for all $t > 0$,

$$\iint_D [|u(x,y,t)|^2+|v(x,y,t)|^2]\,dxdy<\varepsilon\;. \tag{3.12b}$$

The definition of linear stability for (2.3) follows from this simply by setting $\delta = 0$ in (3.6). In either case, note that this definition of stability allows for some (bounded) growth of perturbations. A perturbation that grows without bound, like what occurs in (2.3), is unstable according to (3.12).

With this definition, it follows from (3.11) that $\mu_0(t)$ in (3.4b) is a linearly stable solution of (2.8). The substitution in (3.6) represents one Fourier mode in a complete set of such modes, and the bound in (3.11) is uniformly valid, for all (*m,l*). Thus if we choose

$$\Delta(\varepsilon)\le \exp\{\frac{8k_0^2\,|A|^2}{\delta}\}\cdot\varepsilon/2 \tag{3.13}$$

and use Parseval's relation (*cf. Guenther and Lee*, 1988), then (3.12) is always satisfied, for any $\varepsilon > 0$. Hence, linear stability for any $\delta > 0$.

Thus, we arrive at the following result.

a) If $\delta = 0$ (*i.e.*, without damping), then the solution $\psi_0(t)$ of (2.3), which solution represents a spatially uniform train of plane periodic waves in deep water, is linearly unstable because one can always find Fourier modes in the unstable region in Figure 2. These Fourier modes grow without bound in the linearized dynamics.

b) If $\delta > 0$ (*i.e.*, with damping), then the solution $\mu_0(t)$ of (2.3), which solution represents a spatially uniform train of plane periodic waves in deep water, is linearly stable by (3.12) and (3.13). Individual Fourier modes can grow, but their growth is limited by (3.11).

See *Segur et al.* (2005) for a separate proof of nonlinear stability.

4. Experiments on stability of uniform wave trains in deep water

The experiments discussed in this section and the next were conducted in a wave channel at Penn State that was 43 ft long, 10 in wide, with a glass bottom and sidewalls. It is not the wave tank shown in Figure 1. The water depth in these experiments was 20 cm. Waves were generated at one end of the tank with a plunger-type wavemaker that oscillated vertically and that spanned the width of the tank. At the other end of the tank was a sanded-glass beach to minimize reflections, but the experiments were conducted as transient experiments that ended before waves had enough time to reflect and return to the test section. The frequency of the carrier wave was 3.33 Hz, and the wavemaker had an exponential cross section to mimic more closely the (linearized) velocity field of a deep-water wave at that frequency.

Waves were measured with a non-intrusive, capacitance-type wave gage that spanned 12.7 cm of the width of the tank, and 6 mm in the direction of wave propagation. See *Segur et al.* (2005) for more information about experimental equipment and procedures.

In each set of experiments, the height η_w of the wavemaker in the undisturbed water level was prescribed to be a modulated sine wave

$$\eta_w(T) = 2\,|a_0|\sin(\omega_0 T)[1+2r\sin(\omega_p T)]\,. \tag{4.1}$$

Here ω_0 is the frequency of the carrier wave, ω_p is the frequency of the modulational perturbation, $2|a_0|$ is the crest-to-trough amplitude of the carrier wave, and r is the ratio of perturbation amplitude to carrier wave amplitude. In each set of experiments, one set of sidebands was seeded initially, as in (4.1). Then other sidebands grew because of nonlinear interactions of the seeded sidebands with the carrier wave.

One set of experiments consisted of N experiments – typically $N = 12$. In the nth experiment of the set ($n = 1,\dots, N$), the wave gage was fixed at $X_n = 128 + 50(n-1)$ cm from the wavemaker, and a time-series of the water surface displacement was measured at that location. The n=1 location was chosen to be out of the region of evanescent waves near the wavemaker.

From each measured time-series, we computed its complex Fourier transform. From the complex Fourier transform at the $n = 1$ location, we obtained initial data for the (linearized) evolution equations of the two seeded sidebands, in (3.8). The solution of those equations predicted the complex amplitude of the two seeded sidebands at each subsequent location.

By making use of (2.8), one can also find weakly nonlinear evolution equations for each of the other sidebands, generated by nonlinear interactions. (See section 5 of *Segur et al.*, 2005.) In addition, from (2.2) one can also predict the evolution of the second harmonic. This prediction provides a serious test of the damped theory, because if the carrier wave decays as $e^{-\delta t}$, then it follows from (2.2) that its harmonic must decay as $e^{-2\delta t}$. In all cases, these predictions have no adjustable parameters.

The validity of the exponential decay model is crucial for the validity of (2.4). We conducted careful experiments to test this decay model. We found that for waves of small or moderate amplitude, wave amplitudes decayed approximately exponentially, and that the decay rate (δ in (2.4)) remained essentially constant for about two hours after we had cleaned the surface.

Therefore we measured δ empirically for each set of experiments, and conducted each set of N experiments within two hours after cleaning the water surface.

Figures 3 and 4 show the output of a typical set of experiments. Each row of the figure shows the measured water surface displacement (in cm), as well as the magnitude of its Fourier transform. In our comparisons we used the full complex Fourier transform, but we plot only the magnitude. For these experiments, $\omega_o = 2\pi(3.33)$, $\omega_p = 2\pi(0.17)$, $k_o = 0.441$/cm, $\varepsilon = 2\,k_o|a_o| = 0.10$, and the measured spatial decay rate was $\bar{\delta} = 0.110/m$. The dimensionless δ used in the theory was then obtained from $\bar{\delta} = \varepsilon^2 k_0 \delta$.

At the first measuring location, X_1, the prominent features are:

- the carrier wave at 3.33 Hz;
- two sidebands resulting from the seeded perturbation at 3.16 and 3.50 Hz;
- the second harmonics near 6.67 Hz.
- the third harmonics near 10 Hz.

As this modulated wavetrain propagated downstream, the amplitudes at these frequencies changed slowly. In addition, other sidebands with frequencies near that of the carrier wave also grew, as predicted by either the nondissipative model in (2.3) or the dissipative model in (2.4). By X_3, there was observable energy in higher-frequency sidebands at about 3.67, 3.84 and 4.02 Hz, and in a lower-frequency sideband at 2.99 Hz. The time series show that the wavetrain evolved due both to an overall decay and to the growth of these sidebands. Nevertheless, the growth of the sidebands was bounded, as predicted by (2.4). In these experiments, no sideband amplitude even grew to half the amplitude of the carrier wave.

The distribution of wave energy in discrete sidebands, as shown in the Fourier transforms in Figures 3 and 4, suggests that it might be useful to represent the solution of (2.8) as a Fourier series. Moreover, our capacitance-type wavegage effectively averages out the y-dependence in the signal, so we can use a one-dimensional Fourier series:

$$<\mu(x,y,t)>=\sum_{-\infty}^{\infty} a_n(t)\cdot e^{inbx}\,, \tag{4.2}$$

where $<\mu>$ represents the y-averaged signal, $a_0(t)$ is the Fourier amplitude of the carrier wave, b is proportional to the frequency difference (ω_p) between the carrier wave and each of the seeded sidebands, $\{a_1(t), a_{-1}(t)\}$ are the Fourier amplitudes of the two seeded sidebands, $\{a_2(t), a_{-2}(t)\}$ are the amplitudes of the next two sidebands, *etc.* In this notation, the equations in (3.8) are equivalent to linearized evolution equations for $\{a_1(t), a_{-1}(t)\}$. One can also develop weakly nonlinear equations for the amplitudes of the higher sidebands (see *Segur et al.*, 2005).

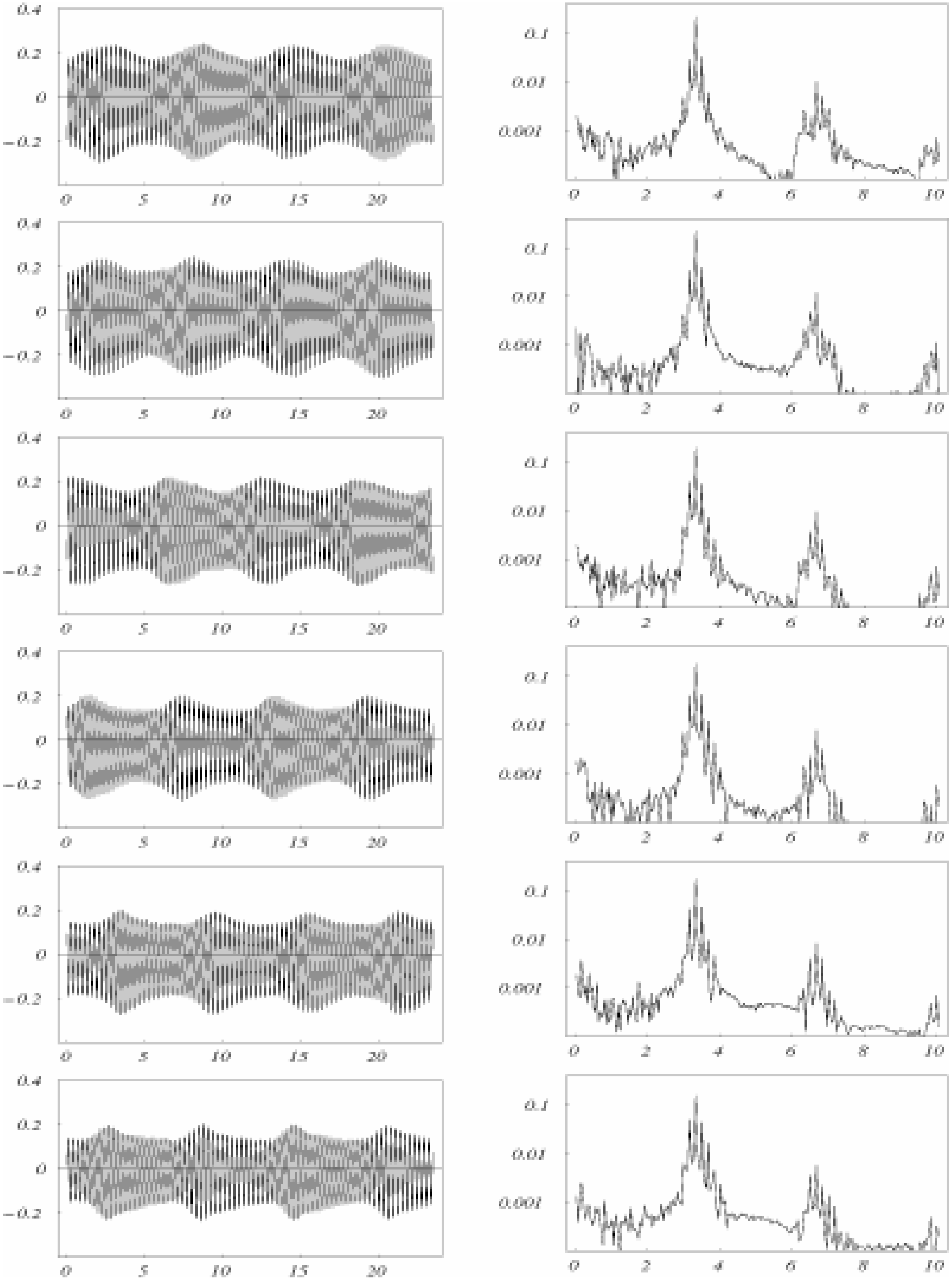

Figure 3. Water surface displacement (cm) as a function of time, and corresponding Fourier coefficients (cm) obtained from 6 experiments when the wave gage was fixed at 128 + 50(n-1) cm from the wavemaker, for (n = 1, 2, 3, 4, 5, 6).

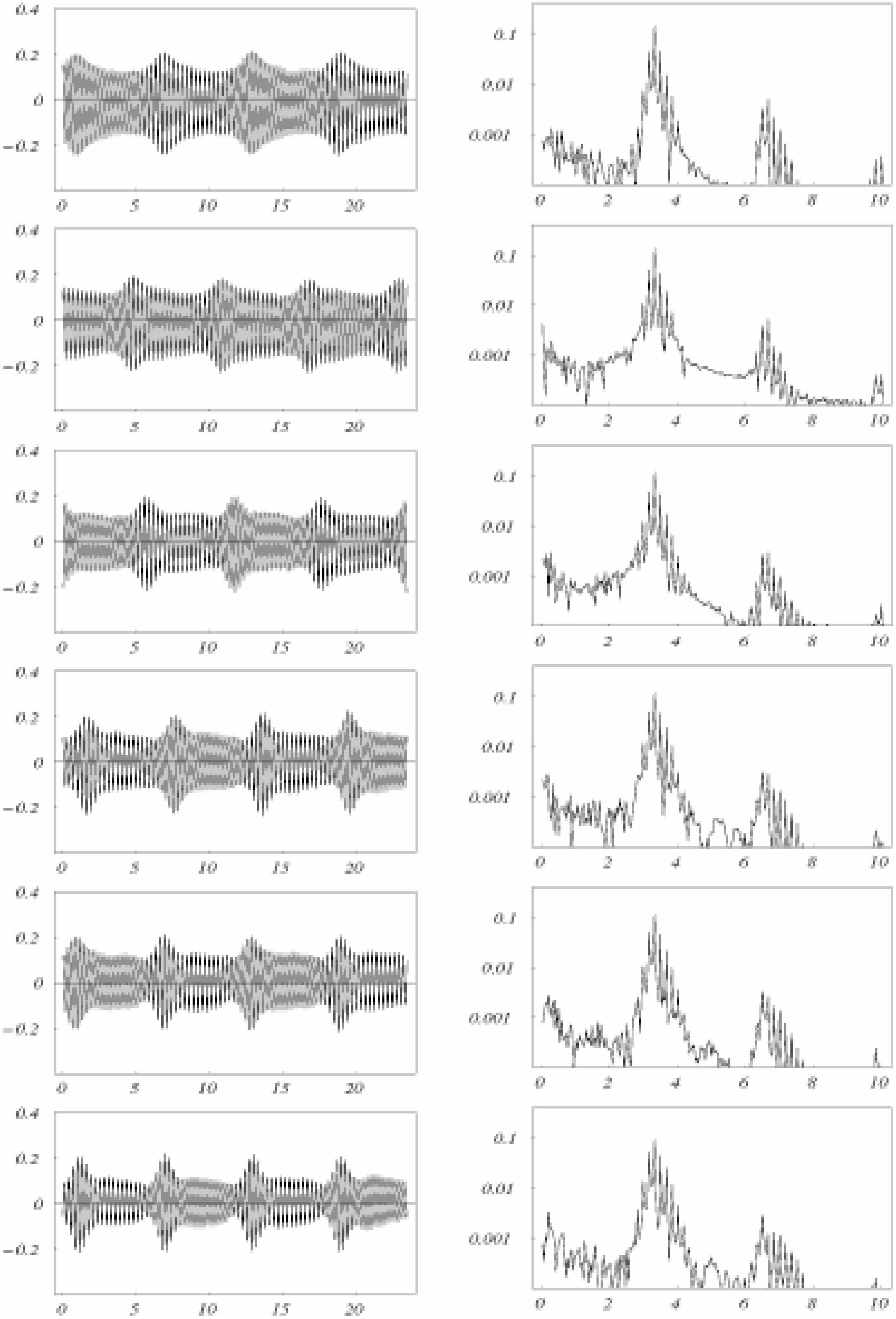

Figure 4. Water surface displacement (cm) as a function of time, and corresponding Fourier coefficients (cm) obtained from 6 experiments when the wave gage was fixed at 128+ 50(*n-1*) cm from the wavemaker (for N=7,8,9,10,11, 12).

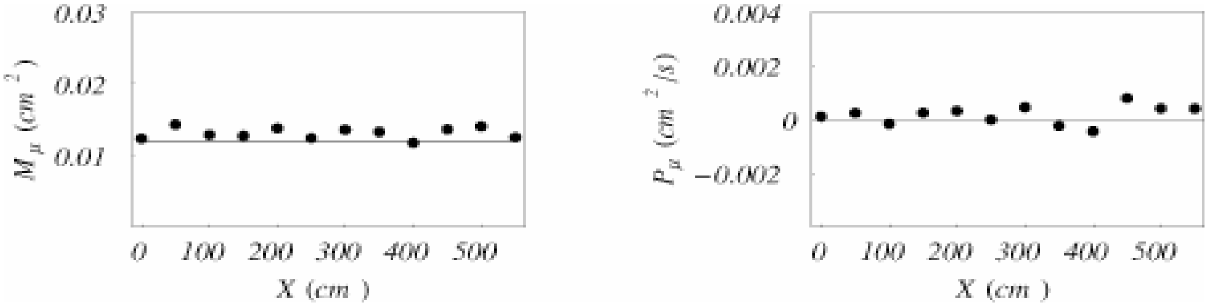

(a) (b)

Figure 5. Measurements (dots) of (a) M_μ and (b) P_μ as functions of distance from the wavemaker. (X=0 cm is 128 cm from the wavemaker.) The line in (a) is simply a horizontal line continued from the first data point.

Next we compare the predicted and observed evolution of the integral quantities from (2.9), the amplitude of the carrier wave (3.33 Hz), the sidebands that resulted from the seeded perturbation (3.16, 3.50 Hz), the second sidebands (2.99, 3.67 Hz), the third sidebands (2.82, 3.84 Hz), and the second harmonic of the carrier second sidebands wave (6.67 Hz). In effect, this list contains every quantity large enough to measure.

For the evolution of wavetrains like those in Figures 3 and 4, (2.4) requires that M_μ and P_μ in (2.9) be constant in the decaying reference frame (i.e., with each measured amplitude magnified by $e^{+\delta t}$, to filter out the overall decay). Figure 5 shows the measured values of the conserved quantities for this set of experiments.

The data have (twice) the decay rate filtered out and are essentially constant. (In effect, we chose the empirical parameter δ for each set of experiments to make M_μ as constant as possible for those experiments.)

In every set of experiments in which M_μ and P_μ were essentially constant, we found that the damped model predicted the experimental data with good accuracy. We also found a class of experiments in which (M_μ,P_μ) were not constant; in these experiments there was downshifting, discussed in §5. Our most reliable criterion for the validity of the damped model in (2.4) was that (M_μ,P_μ) were essentially constant as the wave train evolved.

Figure 6 shows the measured and predicted amplitudes of the set of seeded sidebands, $\{a_{-1}(t), a_1(t)\}$. In Figures 6, 7, and 8a, each measured amplitude is magnified by $e^{+\delta t}$ to filter out the overall decay, where δ was deduced from measured values of $M(t)$, as described above. The measured amplitudes in Figure 6 have errors of ± 0.001 cm. The predicted values of the amplitudes (solid curves) were obtained by integrating (3.8) numerically, starting with measured initial values based on the (complex) values of $\{a_{-1}(0), a_1(0)\}$ measured at the n=1 location. The dashed curves show the growth predicted by Benjamin & Feir (1967). In the comparisons of theory and experiment shown in Figure 6 and in all of the subsequent comparisons, *no free parameters* were available to help fit the data.

The comparison in Figure 6 is probably the most important comparison in this paper. The figure shows that for short "times" (*i.e.*, for approximately 1 m down the tank in these experiments), the damped theory (solid curve), undamped Benjamin-Feir theory (dashed curve), and measured data all agree. For longer times, decay of the carrier wave slows the growth rate of the sidebands, as observed in the data and in the damped theory, but not in the undamped theory. Recall that the undamped theory is being compared to data that has had the damping factored out. So, Figure 6 shows that correcting the inviscid growth rate by subtracting the decay rate from it is inadequate for these waves.

Over the duration of these experiments, the damped theory predicts the measured growth of the sidebands from their starting values with reasonable accuracy. Equation (3.8) predicts that this growth must eventually stop completely. Continuing the computation of (3.8) beyond 6 m, one finds that $|a_{-1}(t)|$ and $|a_1(t)|$ would have achieved maximum amplitudes of about 0.18 cm, or about 5.5 times their initial amplitudes, at about 10.7 m downstream from the wave-maker. We ended our experiments before that distance to minimize the effects of reflections from the beach. As a result, the predicted upper bound on growth of the seeded sidebands is not evident in this set of experiments. In other experiments, not shown here (see Figure 9 of *Segur et al*, 2005), the growth of the sidebands ended within the test section of the experiments.

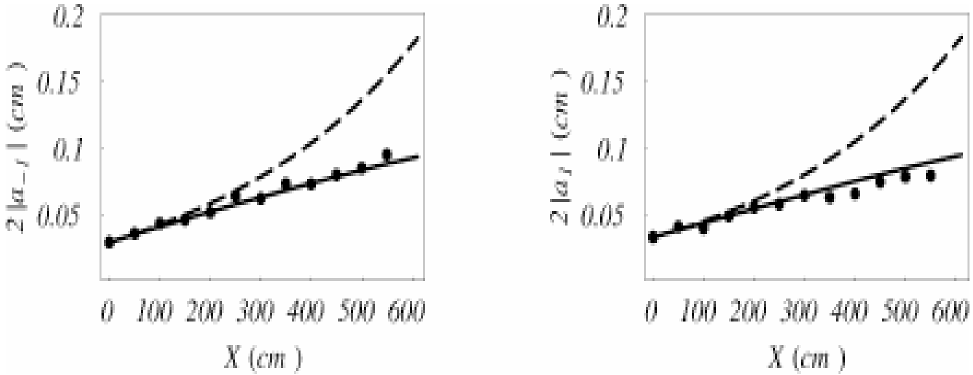

Figure 6. Predictions (solid curves) from (3.8) and measurements (dots) of the amplitudes of the two seeded sidebands, $|a_{-1}|$ and $|a_1|$, as functions of distance from the wavemaker. (X=0 cm is 128 cm from the wavemaker.) Measured values were taken from Figures 3 and 4, but amplified by $e^{+\delta x}$ to filter out the overall decay. The dashed curves show the classic Benjamin-Feir (1967) prediction of constant growth rate.

Figure 7 shows the growth of the next two sets of sidebands, $\{a_{-2}, a_2, a_{-3}, a_3\}$. None of these sidebands was seeded, so they started with smaller amplitudes than $\{a_{-1}, a_1\}$, and they remained smaller. The predicted values for these complex amplitudes were obtained by integrating numerically weakly nonlinear evolution equations obtained from (2.8), starting from initial values measured at the $n = 1$ location. As in Figure 6, the damped theory predicts the observed data over the duration of the experiment with good accuracy, and with no free parameters. The predictions for all six sidebands are in fairly good agreement with the data, which have errors of ± 0.001 cm. Note that $|a_2(t)|$ grows nearly twice as much as $|a_{-2}(t)|$ during the experiments, and similarly with $|a_3(t)|$ and $|a_{-3}(t)|$. Equation (2.8) accurately predicts this asymmetric growth. Equation is symmetric under $\{x \to -x\}$, but Figure 7 shows that (2.8) admits solutions with growing asymmetry. What is needed is that the initial data $\{a_{-2}(0), a_2(0)\}$ be asymmetric. Then the asymmetric part of the solution grows for awhile. The same situation holds for $\{a_{-3}, a_3\}$.

One can work out from (2.8) predictions of how the carrier wave and its second harmonic evolve. Figure 8 shows the comparison of these predictions with the measured evolution. Figure 8a shows the measured values of the carrier wave amplitude obtained from the Fourier transforms, with the overall decay rate filtered out. This amplitude varies slowly in this reference frame as it loses energy to the sidebands.

Figure 8b shows the measured and predicted evolution of the second harmonic of the carrier wave. Recall from (2.2) that the second harmonic decays with twice the decay rate of the carrier wave. Thus, twice the usual decay rate has been factored out in Figure 8b. The dots in Figure 8b are the measured amplitudes of the harmonic, magnified by $e^{2\delta t}$. The curve shows the predicted evolution of the second harmonic, taking into account the evolution of the carrier wave and the first set of sidebands.

Note that the vertical scale in Figure 8b is finer than that in 8a; thus, 8b shows that (2.2) predicts the evolution of the harmonic quite accurately. *Lake and Yuen* (1977) found that (2.2) did not predict accurately the measurements in their experiments, but we found no such problems.

This completes our comparisons of the predictions from the damped model (2.8) with experimental data. Figures 5-8 show that (2.8) predicts all the easily measured features of the data shown in Figures 3 and 4 with good accuracy, using no adjustable parameters. Even so, this good agreement does not rule out the possibility that another theory might also predict these data accurately. For example, it is known that the initially exponential growth rate, predicted by *Benjamin and Feir* (1967) and shown in Figure 6, can last only until nonlinear interactions among sidebands become important. For longer times, (2.3) predicts that the growth of the seeded sidebands, $\{\alpha_1, \alpha_{-1}\}$,must diminish as these growing modes begin to lose energy to higher sidebands.

Thus even with no damping, ($\delta = 0$), a nonlinear theory like (2.3) also predicts that the initially vigorous growth of unstable sidebands must eventually slow down, consistent with the behaviour shown in Figure 6. In terms of the behaviour of $\{\alpha_1, \alpha_{-1}\}$, the differences between the two theories are these:

(i) the mechanism for the slowing down is different (nonlinear interactions for (2.3) *vs*. damping of the carrier wave for (2.4)); and

(ii) the time-scales on which this slowing down occurs are typically different.

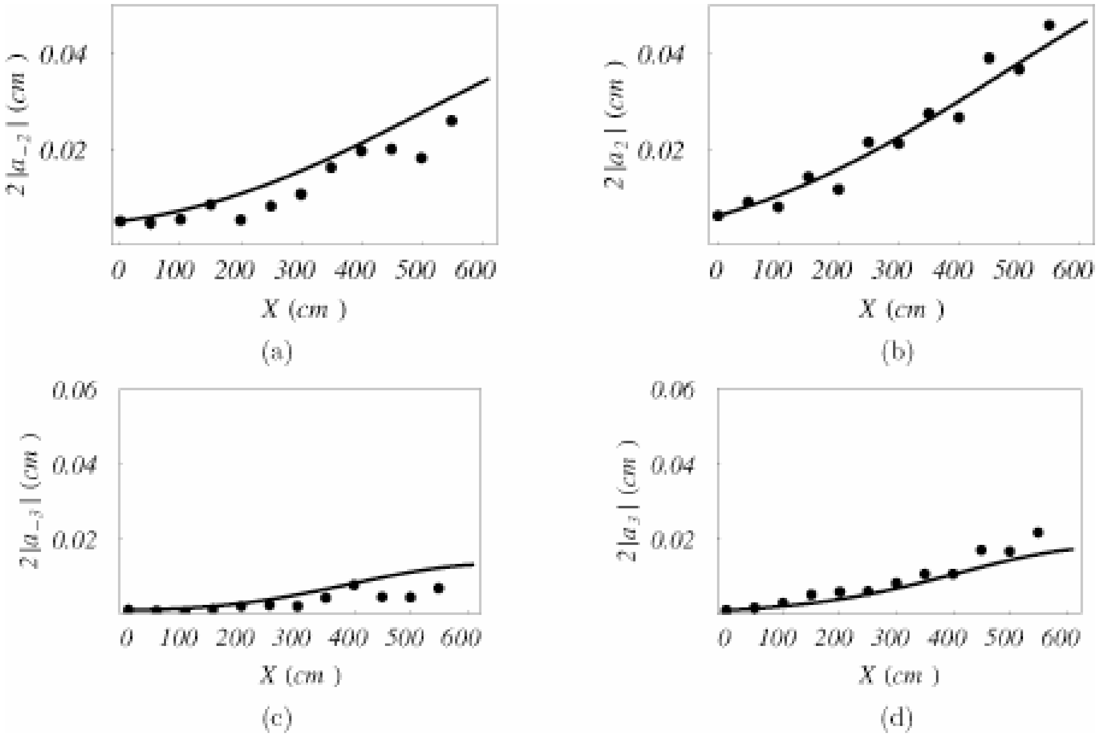

(a) (b)

(c) (d)

Figure 7. Predictions (solid curves) inferred from (2.8) and measurements (dots) of the amplitudes of the second set of sidebands, (a) $|a_{-2}|$ and (b) $|a_2|$, and the amplitudes of the third set of sidebands, (c) $|a_{-3}|$ and (d) $|a_3|$, as functions of distance from the wavemaker. (X=0 cm is 128 cm from the wavemaker.) Measured values were taken from the data of Figures 3 and 4, but amplified by $e^{+\tilde{\delta}X}$ to filter out the overall decay.

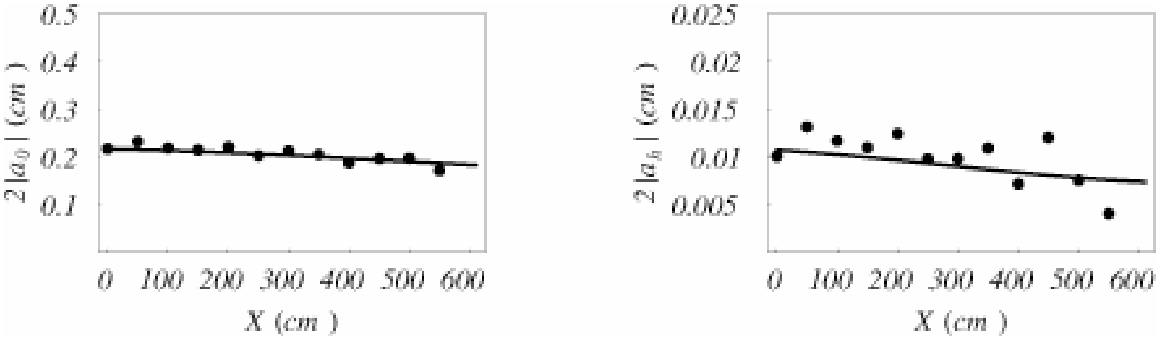

(a) (b)

Figure 8. Results for (a) the carrier wave amplitude and (b) its second harmonic as functions of distance from the wavemaker. (*X*=0 cm is 128 cm from the wavemaker.) The solid curve in (a) is the prediction based on (2.8); the dots are the measured Fourier amplitudes at the carrier wave frequency, but amplified by $e^{+\tilde{\delta}X}$. The solid curve in (b) is the prediction based primarily on (2.2). The dots are the measured Fourier amplitudes at twice the carrier wave frequency, amplified by $e^{+2\tilde{\delta}X}$.

Dysthe's (1979) model could also be used to predict the evolution shown in Figures 3 and 4. He derived his higher-order correction to (2.3) in order to predict the behaviour of nonlinear events more accurately. In the form given by *Lo and Mei* (1986), using the notation given herein, Dysthe's model in one spatial dimension can be written as

$$\begin{aligned} i\partial_t\psi - \partial_x^2\psi - 4k_0^2\,|\psi|^2\,\psi - 32i\varepsilon k_0^2\,|\psi|^2\,\partial_x\psi \\ +16\varepsilon k_0^2\partial_x\phi(|\psi|^2)\cdot\psi = 0 \end{aligned} \tag{4.3}$$

where

$$\partial_x\phi(f) = -\frac{1}{4\pi}\int |k|\cdot\hat{f}(k,t)e^{ikx}dk,$$

$$f(x,t) = \frac{1}{2\pi}\int \hat{f}(k,t)e^{ikx}dk,$$

and $\varepsilon = 2k_0|a_0(0)|$. *Lo and Mei* (1986) showed that (4.3) predicts the evolution of some narrow-banded wave packets in deep water more accurately than does (2.3).

We do not show the comparison here, but *Segur et al.* (2005) used (4.3) to predict the evolution of $\{a_0, a_{-1}, a_1, a_{-2}, a_2, a_{-3}, a_3\}$ as functions of time. For the experiments shown in Figures 3 and 4, the results between NLS (2.3) and the NLS with higher-order terms (4.3) were almost indistinguishable for most of the Fourier amplitudes. For this set of experiments, the damped NLS model, (2.4) or (2.8), predicts the evolution of every measured amplitude much more accurately than either of the undamped models, (2.3) or (4.3). This striking discrepancy in accuracy among these three mathematical models illustrates one of our main points. Equations (2.3) and (4.3) both predict that unstable sidebands stop growing after their amplitudes become large enough that nonlinear interactions among sidebands become dynamically important. Equation (2.4) provides another option: damping of the carrier wave can slow and eventually stop the growth of the unstable sidebands altogether, before their amplitudes become large enough that nonlinear interactions play a role. When this happens, sideband amplitudes always remain small, and the difference between nonlinear terms in (2.3) and (4.3) has little effect on the evolution of the wavetrain. For the experiments shown in Figures 3 and 4, damping controls the growth of the sidebands, precluding serious nonlinear effects.

5. Frequency downshifting

Aside from issues of stability, a second process in deep water in which dissipation apparently plays an important role is frequency downshifting, first observed by *Lake et al*., (1977). Figure 9 shows an example of a modulated train of nearly periodic waves that downshifts in deep water. This set of experiments was comparable to those shown in Figures 5-8 in many respects:

- the frequency of the carrier wave was 3.33 Hz;
- the frequency of the modulating perturbation was 0.17 Hz;
- the dimensionless amplitude of the carrier wave was $\varepsilon = 2\ k_o|a_o| = 0.093$ (instead of 0.10 for the previous set of experiments); and
- the measured spatial decay rate $\bar{\delta}$ was about 0.105/m (instead of 0.110/m for the previous experiments).

The main difference was that the perturbation carried more energy in these experiments – the amplitudes of the seeded sidebands here were about twice as big as those in Figures 3 and 4. Figure 9(a) shows a modulated train of periodic plane waves that was measured at the first gage location. The Fourier transform of the initial wave shape is shown in (b), where the carrier wave frequency is marked. Also evident in (b) are the two sidebands that contain the input modulation (at 3.16 Hz and 3.50 Hz), second sidebands generated by nonlinear interactions among the carrier wave and the input sidebands (at 2.99 Hz and 3.67 Hz), and second harmonics of these waves, near 6.67 Hz.

Figure 9(c) shows the wave pattern after it has propagated 550 cm (about 39 wavelengths of the carrier wave) down the channel, and (d) shows the Fourier transform of that signal. It is evident from (c) that the wave pattern has evolved significantly during this time, including both growth of sidebands and an overall loss of energy. Figure 9(d), which shows the Fourier transform of the signal in (c), also shows that the peak frequency has shifted from 3.33 Hz down to 3.16 Hz. This is an example of downshifting.

Recall from (2.5) that the NLS model, (2.3) admits integral quantities that are constants of the motion. In what follows, we are primarily interested in M, and in the x-component of $\boldsymbol{P}$:

$$P_x = \frac{i}{A_D}\iint_D[\psi\partial_x\psi^* - \psi^*\partial_x\psi]dxdy \tag{5.1}$$

Because $|\psi|^2 \geq 0$ and M = constant, one can interpret $|\psi|^2$ as a non-normalized probability density. In addition, because x represents actual time in the coordinates used in (2.3), one can interpret the ratio $\{P_x/M\}$ as the *average frequency of the wave train*.

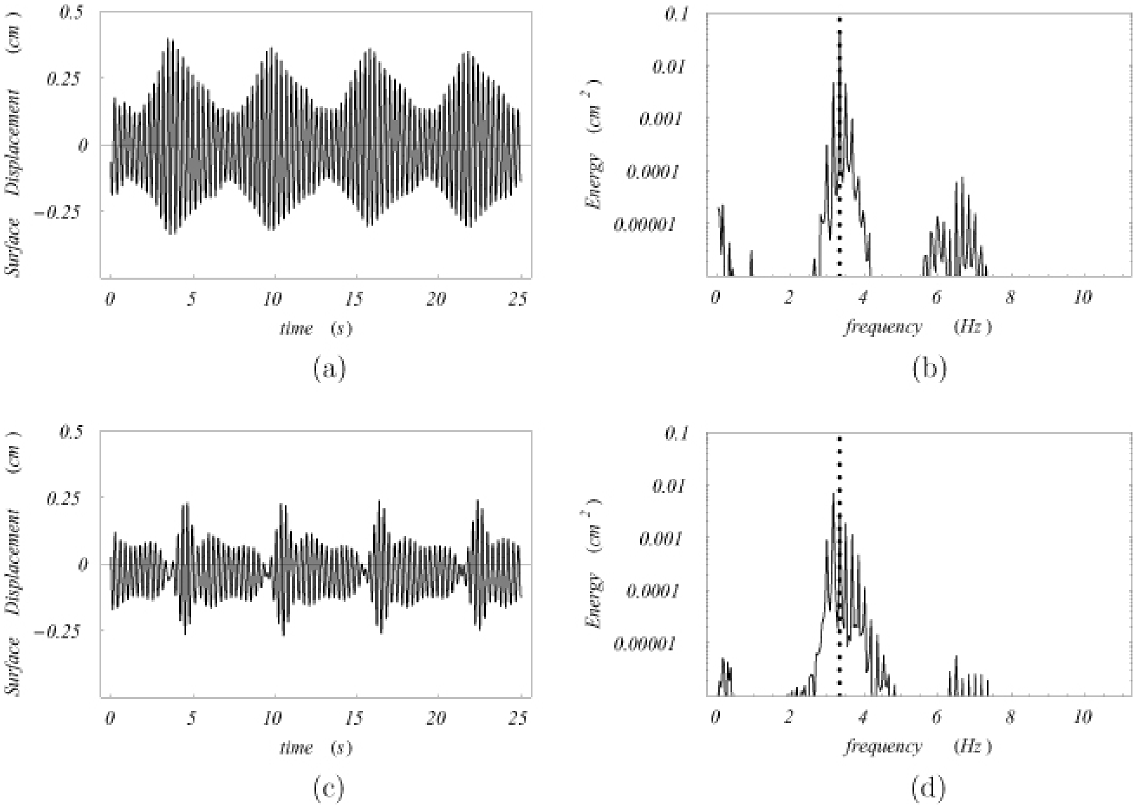

(a) (b)

(c) (d)

Figure 9. Water surface displacement measured slightly downstream of the wavemaker in (a), and 550 cm further downstream in (c). The Fourier transforms of these signals are shown in (b) and (d), respectively. The vertical lines in (b) and (d) show the location of the carrier wave frequency (3.33 Hz).

Following *Gordon* (1986) and *Trulsen and Dysthe* (1997), we say that a wavetrain experiences frequency downshifting when $\{P_x/M\}$ decreases monotonically in "time" (i.e., in distance down the tank). Then it follows that the NLS model can never predict downshifting, because $\{P_x/M\}$ is constant according to (2.3). This was already known. For the same reason, its higher order version (4.3) cannot predict downshifting either.

The damped model in (2.4) does no better than the undamped model in (2.3) at explaining downshifting. For (2.4) with $\delta > 0$, the integral quantities defined in (3.3) and (5.1) vary in a simple way:

$$M(t) = M(0)\cdot\exp(-2\delta t)$$
$$P_x(t) = P_x(0)\cdot\exp(-2\delta t)\ .$$

Thus, $M(t)$ and $P_x(t)$ each vary in time according to (2.4), but their ratio $\{P_x/M\}$ is constant in time. So (2.4) also predicts no downshifting.

Figure 10 shows the measured evolution of these integral quantities as the wave propagates, for the experiments featured in Figure 9. As required by (2.4), $M(t)$ varies approximately exponentially. But contrary to (2.4), $P_x(t)$ does not decay towards zero, and $\{P_x/M\}$ is certainly not constant. Apparently downshifting requires a more complicated model than any of (2.3), (2.4), or (4.3).

It might be worthwhile to comment on two other theoretical models that have been proposed to explain frequency downshifting. Downshifting has been observed not only for waves in deep water, but also for electromagnetic waves in an optical fiber. *Gordon* (1986) proposed an explanation of downshifting in an optical fiber in terms of a Raman effect, in which the (very high frequency) electromagnetic wave interacts resonantly with the natural vibrations of molecules that make up the optical fiber. The EM wave loses energy to the molecules, so this amounts to a dissipative process as far as the EM wave is concerned, but the form of dissipation is more complicated than that in (2.4). Regardless of the validity of this model for optical waves, we have been unable to identify an analogue of the Raman effect for waves in deep water. Further, the empirical addition of the Raman term to the damped NLS equation does not predict our experimental results.

Separately, *Trulsen and Dysthe* (1997) proposed a higher-order NLS model, which they claim exhibits frequency downshifting. Our research group has some

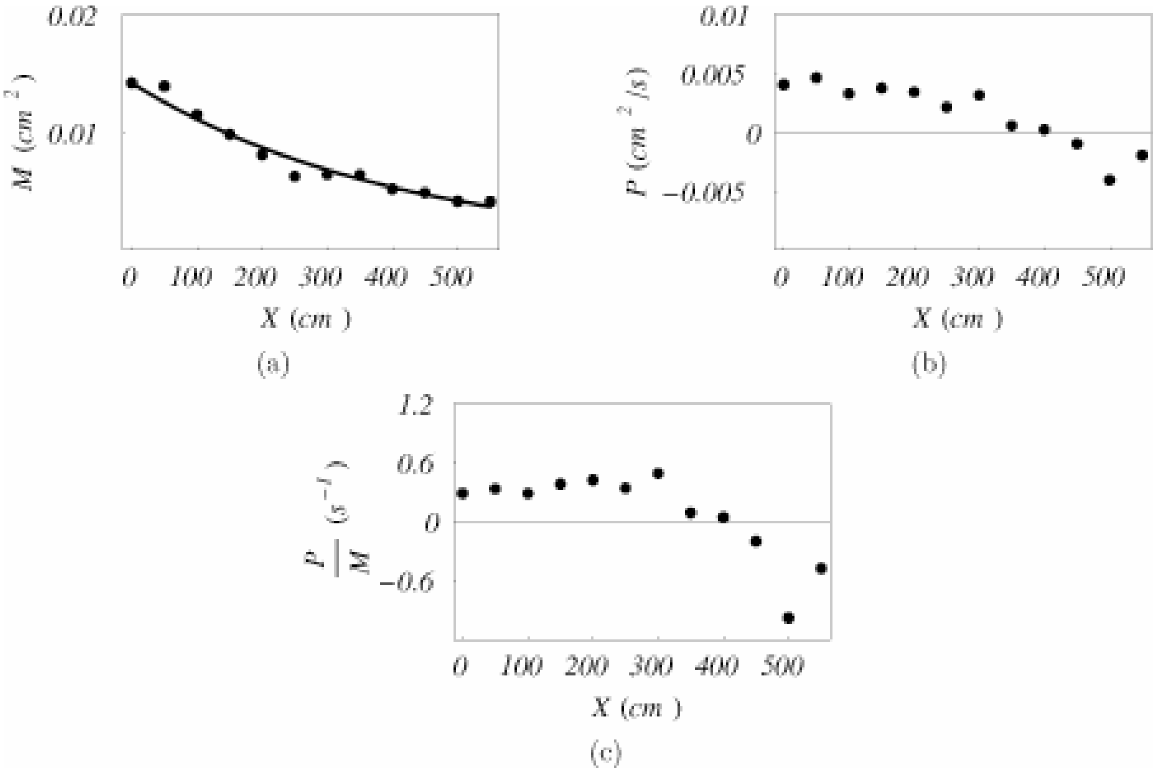

Figure 10. Integral quantities, (a) $M(t)$, (b) $P_x(t)$, and (c) their ratio, for the experimental data shown in Figure 9.

questions about their model, including the observation that their model seems not to be variational (Deconinck, private communication). We find it troubling that the well-known equations for inviscid water waves can be derived from a Lagrangian (*Luke*, 1967), and so can the nonlinear Schrödinger equation, but the model of *Trulsen and Dysthe* (1997), which should sit between these two in a hierarchy of approximate models, cannot be derived from a Lagrangian. Because of these difficulties, we regard downshifting as a dissipative process that is still not understood. We grant that others might see this issue differently at this time.

6. Rogue waves

We conclude by returning to the subject of these Proceedings: rogue waves. Our recent work has identified some shortcomings of the usual NLS model for waves in deep water, because it neglects dissipative effects that have a stronger influence on issues like stability than had been recognized before. We have no experimental evidence about whether dissipation might also affect the early development of rogue waves.

Acknowledgments: We are grateful to Peter Müller for the invitation to participate in Aha Workshop. We are also grateful to him for pointing out that our recent work might be relevant to rogue waves. The work described here was funded in part by the National Science Foundation, under grants DMS-9972210, DMS-0139742, DMS-0139847, and by Packard and Sloan Fellowships.

References

Ablowitz, M. J., and Segur, H., 1981, *Solitons and the Inverse Scattering Transform*, SIAM, Philadelphia, 391 pp.

Benjamin, T. B., and Feir, J. E., 1967, The disintegration of wavetrains in deep water, Part 1, *J. Fluid Mech.*, **27**, pp. 417-430.

Bleymaier, M., Henderson, D., and Segur, H., Stable, three-dimensional wave patterns in deep water, in preparation

Dysthe, K., 1979, Note on a modification to the nonlinear Schrodinger equation for application to deep water waves, *Proc. Roy. Soc.,A*, **369**, pp. 105-114

Gordon, J. P., 1986, Theory of the soliton self-frequency shift, *Optics Lett.*, **11**, pp. 662-664.

Guenther, R. B., and Lee, J. W., 1988, *Partial Differential Equations of Mathematical Physics and Integral Equations,* Dover, N.Y., 557 pp.

Hammack, J. L., Henderson, D. M., and Segur, H., 2005, Deep-water waves with persistent, two-dimensional surface patterns, *J. Fluid Mech.*, **532**, pp. 1-51.

Ince, E. L., 1956, *Ordinary Differential Equations*, Dover, N.Y., 558 pp.

Lake, B. M., Yuen, H. C., Rungaldier, H., and Ferguson, W. E., 1977, Nonlinear deep-water waves: theory and experiment. Part 2. Evolution of a continuous wave train, *J. Fluid Mech.*, **83**, pp. 49-74.

Lo, E., and Mei, C.C., 1985, A numerical study of water-wave modulations based on a higher-order nonlinear Schrodinger equation, *J. Fluid Mech.*, **150**, pp. 395-416.

Luke, J. C., 1967, A variational principle for a fluid with a free surface, *J. Fluid Mech.*, **27**, pp. 395-397.

Miles, J. W., 1967, Surface-wave damping in closed basins, *Proc. Roy. Soc. A*, **297**, pp. 459-475.

Nemytskii, V. V., and Stepanov, V.V., 1960, *Qualitative Theory of Differential Equations*, Princeton University Press, Princeton, N.J., 519 pp.

Segur, H., Henderson, D. M., Carter, J., Hammack, J., Li, C-M, Pheiff, D., and Socha, K., Stabilizing the Benjamin-Feir Instability, *J. Fluid Mech*, to appear.

Stokes, G. G., 1847, On the theory of oscillatory waves, *Trans. Cambridge Phil. Soc.*, **8**, p. 441. Also in *Mathematical and Physical Papers*, **1**, pp. 197-229

Sulem, C., and Sulem, P.L., 1999, *The nonlinear Schrodinger equation*, Springer, New York, 345 pp.

Trulsen, K., and Dysthe, K. B., 1997, Frequency downshift in three-dimensional wave trains in a deep basin, *J. Fluid Mech.*, **352**, pp. 359-373.

Zakharov, V. E., 1968, Stability of periodic waves of finite amplitude on the surface of a deep fluid, *J. Appl. Mech. Tech. Phys.*, **2**, pp. 190-194.